Inorganic Chemistry
Article

Inorg. Chem. **2009**, *48*, 9671–9683 **9671**
DOI: 10.1021/ic900386q

Structure and Properties of Alkali Cobalt Double Oxides $A_{0.6}CoO_2$ (A = Li, Na, and K)

Michaël Pollet,* Maxime Blangero, Jean-Pierre Doumerc, Rodolphe Decourt, Dany Carlier, Catherine Denage, and Claude Delmas

CNRS, Université de Bordeaux, ICMCB, 87 Avenue du Dr. A. Schweitzer, Pessac, F-33608, France

Received February 25, 2009

Lamellar A_xCoO_2 cobalt double oxides with A = Li, Na, and K ($x \sim 0.6$) have been synthesized and their chemical (alkali content, oxidation state, and structure) and physical (resistivity, thermopower, magnetization, and specific heat) properties have been studied. All the three materials exhibit strong electron correlation emphasized by their behavior ranging from Fermi liquid to spin-polarized system. Our results show that both the dimensionality of the interactions and the nature of the alkali play a determining role on the properties.

Introduction

Lamellar A_xCoO_2 cobalt double oxides, where A is an alkali, can accommodate various packing schemes depending on A, its content (x), and the synthesis conditions. The Na_xCoO_2 family in particular has recently regained interest with the discovery of magnetic orders[1] and high thermoelectric properties for the P2-type phases ($x \sim 0.6-0.8$).[2,3] The origin of the large thermopower in these metallic cobalt double oxides is still debated: in a classical approach to the metal,[4,5] it would arise from the band structure features while in the case of strong electron correlations,[6,7] it would be due to the carriers' entropy enhancement. Huang et al.[8] have described the evolution of the structure and physical properties in P2$-Na_xCoO_2$ during the deintercalation of Na^+. In these cobalt double oxides, the carrier concentration within the CoO_2 layers is controlled by the sodium rate in the interslab. This situation is typical of the so-called bronze systems and is also close to the one of high T_c superconductors for which a charge reservoir gives electrons to the CuO_2 sheets.[9] In $Bi_2Sr_2CaCu_2O_{8+\delta}$ and $Ca_{2-x}Sr_x$-RuO_4 superconductors, the electronic perturbations arising from doping are more and more recognized as a source of electronic inhomogeneities at a nanometric scale, directly affecting the physical properties of the system.[10,11] These results thus raise fundamental questions like the links between the electronic degrees of freedom (spin, charge, orbital) and the structural ones (nature, site, symmetry, and distribution of the alkali).[12] To assess this question, we have studied the effect of the nature of the alkali (lithium, sodium, and potassium) on the properties of our materials. Several theoretical works have already been reported on the effect of the interslab but mostly treating it in a mean field approximation, equally considering the details of the alkali. Recently, Lee and Pickett[13] have however reported a first work dealing with the differences between K and Na in half filled alkali cobalt oxides. They have attributed the differences in the behavior mostly to the chemical rather than the structural difference. Namely, the higher ionicity of K seems to be the most discernible difference between their materials. In this work, we extend the discussion to the lithium case and consider a higher alkali content, closer to the conditions required for high thermoelectric properties. Three phases A_xCoO_2 with $x \sim 0.6$ have been synthesized and characterized with A = Li (O3), Na (P′3), and K (P2), where O3, P′3, and P2 refer to the nomenclature introduced by Fouassier et al. to describe the stacking of the CoO_2 slabs along the c axis.[14] The choice for $x \sim 0.6$ is a compromise between the maximum alkali filling

*To whom correspondence should be addressed. E-mail: pollet@icmcb-bordeaux.cnrs.fr.

(1) Sugiyama, J.; Itahara, H.; Brewer, J. H.; Ansaldo, E. J.; Motohashi, T.; Karppinen, M.; Yamauchi, H. *Phys. Rev. B* **2003**, *67*, 214420.
(2) Molenda, J.; Delmas, C.; Hagenmuller, P. *Solid State Ionics* **1983**, *9−10*, 431.
(3) Molenda, J.; Delmas, C.; Dordor, P.; Stoklosa, A. *Solid State Ionics* **1984**, *12*, 473.
(4) Singh, D. J. *Phys. Rev. B* **2000**, *61*, 13397.
(5) Takeuchi, T.; Kondo, T.; Takami, T.; Takahashi, H.; Ikuta, H.; Mizutani, U.; Soda, K.; Funahashi, R.; Shikano, M.; Mikami, M.; Tsuda, S.; Yokoya, T.; Shin, S.; Muro, T. *Phys. Rev. B* **2004**, *69*, 125410.
(6) Koshibae, W.; Tsutsui, K.; Maekawa, S. *Phys. Rev. B* **2000**, *62*, 6869.
(7) Chaikin, P. M.; Beni, G. *Phys. Rev. B* **1976**, *13*, 647.
(8) Huang, Q.; Foo, M. L.; Pascal, R. A.; Lynn, J. W.; Toby, B. H.; Tao He; Zandbergen, H. W.; Cava, R. J. *Phys. Rev. B* **2004**, *70*, 184110.
(9) Cava, R. J. *Science* **1990**, *247*, 656.
(10) McElroy, K.; Lee, J.; Slezak, J. A.; Lee, D. H.; Eisaki, H.; Uchida, S.; Davis, J. C. *Science* **2005**, *309*, 1048.
(11) Zhang, J.; Ismail, R. G.; Moore, S. C.; Wang, H.; Ding, R.; Jin, D.; Mandrus; Plummer, E. W. *Phys. Rev. Lett.* **2006**, *96*, 66401.
(12) Dagotto, E. *Science* **2005**, *309*, 257.
(13) Lee, K.-W.; Pickett, W. E. *Phys. Rev. B* **2007**, *76*, 134510.
(14) Fouassier, C.; Delmas, C.; Hagenmuller, P. *Mater. Res. Bull.* **1975**, *10*, 443.

Published on Web 09/21/2009

rate ($x \sim 0.67$ for potassium compounds[15]), the proximity of an ordered arrangement of the alkalis ($x = 4/7$[17]) to discuss the possible effect of the ordering and the possibility to reach high thermoelectric properties.

Experimental Section

Synthesis of the Compounds. The P′3−Na_xCoO_2 bronzes are obtained form a mixture of Na_2O and Co_3O_4. The nominal composition includes a 10 wt % excess in Na_2O to compensate for the losses in sodium by volatilization and to reach the desired stoichiometry.[16] The mixture is then heated in a gold boat at 550 °C during 12 h. The resulting product is cooled down to 300 °C at a 2 K/min rate and then quenched in a dry atmosphere. The P2−K_xCoO_2 bronzes are obtained from a mixture of KOH and Co_3O_4. The high volatility of the by-product K_2O requires a KOH excess of 17 wt % to obtain the expected composition. The reaction is carried out at 600 °C during 15 h under a dry oxygen flow. The system is then slowly (1 K/min) cooled down to 300 °C and then quenched in the same conditions. Two kinds of phases can be obtained in this way: a disordered phase and an ordered one previously described.[17] After quenching, both sodium and potassium cobalt double oxides are stored in a dry glovebox to prevent any moisture contamination.

The synthesis of the O3−Li_xCoO_2 phase requires two steps: first, a synthesis of the stoichiometric O3-$LiCoO_2$ by conventional solid state reaction and then an electrochemical deintercalation of the lithium ions. Stoichiometric O3-$LiCoO_2$ is prepared by direct reaction of Li_2CO_3 (Alpha Aesar) and Co_3O_4 (prepared by thermal decomposition of $Co(NO_3)_2$-$6H_2O$ from Sigma-Aldrich ACS reagent, containing less than 10 mg/kg of Fe, Ni, or Cu and less than 20 mg/kg of Mn). Li_2CO_3 and Co_3O_4 were mixed in stoichiometric amounts and first reacted for 12 h at 600 °C under oxygen, and then the product was re-ground and heated at 900 °C under oxygen for 15 days. Such a procedure avoids any lithium overstoichiometry and leads to a stoichiometric sample as confirmed by ^{7}Li MAS NMR (Magic Angle Scattering−Nuclear Magnetic Resonance).[18]

The second step requires charging a battery with metallic lithium sheet as negative electrode, $LiCoO_2$ as positive one, and 1 M $LiPF_6$ in (EC/PC/DMC) as electrolyte. We ran GITT experiments on a pellet of standard $LiCoO_2$ without additive, sintered at 800 °C for 24 h under O_2. A low charging rate (C/400, i.e 400 h are required to remove 1 mol of Li^+ ions) was used for charging periods of 109 min. These periods are followed by relaxation periods with $\Delta V/\Delta T = 1$ mV/h as voltage stability criterion for its end (Figure 1). As shown in the inset of Figure 1, at the very end of the deintercalation, a steady state is observed and a homogeneous O3−$Li_{0.6}CoO_2$ phase is obtained.

Characterization Procedures. Elemental analysis of the products was performed by inductively coupled plasma−atomic emission spectrometry (ICP-AES). The average oxidation state of cobalt was determined by iodometric titration.

The X-ray diffraction (XRD) patterns were recorded on a Philips X'Pert Pro powder diffractometer in the Bragg−Brentano geometry, using either Cu or Co Kα radiations. The data collections were made in the 10−120° 2θ range with a 0.0084° step, using an X'Celerator detector (linear PSD covering 2.122 mm). The powders were put in a specific airtight holder under dry argon to prevent any reaction with air moisture. The diffraction data were analyzed using the Rietveld technique[19] as implemented in the Fullprof program.[20] Peak shape was described by a pseudo-Voigt function, and the background level was fitted with linear interpolation between a set of given points with refinable heights. The anomal atomic diffusion factors were corrected for the cobalt anticathode according to the international tables.[21] The alkali site-occupancies were fixed to the values obtained from ICP-AES.

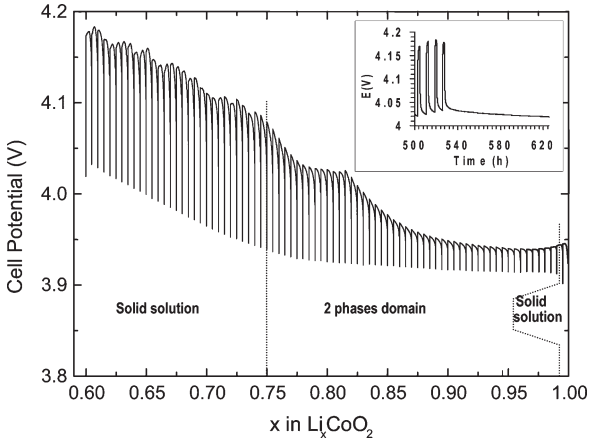

Figure 1. Charge curve near the thermodynamic equilibrium (OCV, Open-Circuit Voltage) of a Li//$LiCoO_2$ battery until $Li_{0.6}CoO_2$ is obtained. (Charge regime: $I = nF/1.44 \times 10^6$, n being the $LiCoO_2$ mole number; Relaxation end criteria is $\Delta V/\Delta T = 1$ mV/h).

Transport properties were measured on cold-pressed pellets, the compactness of which was close to 70%. Electrical direct current (DC) conductivity measurements were performed with the aligned four-probe method[22] in the 4.2−300 K range. Thermoelectric power measurements were performed with a homemade equipment previously described.[23]

Zero field cooled (ZFC) and field cooled (FC) DC-magnetization data in an applied field up to 4 T were collected on a superconducting quantum interference device magnetometer (Quantum Design) in the 2−350 K temperature range.

Specific heat data were collected between 1.8 and 400 K on a Quantum Design Physical Properties Measurement System (PPMS) using the 2-τ relaxation method.

Results

Chemical Analysis. The results obtained using ICP-AES on all the three A_xCoO_2 (A = Li, Na, and K) phases are shown in Table 1. The alkali contents calculated from the A/Co ratio are very close to $x = 0.6$. The average oxidation states determined by iodometric titration are also listed in the same table. Except in the sodium case,[24] the results are in reasonable agreement with the values expected from electroneutrality. The lower average oxidation state observed in the sodium phase is in agreement with the results of other groups. For

(15) Delmas, C.; Fouassier, C.; Hagenmuller, P. *J. Solid State Chem.* **1975**, *13*, 165–171.
(16) Butel, M. *Etude de nouveaux oxyhydroxydes de cobalt pouvant être utilisés comme additif conducteur électronique ajoutés à l'hydroxyde de nickel dans les accumulateurs nickel/cadmium et nickel/métal hydrure*. Ph.D. Thesis, Université de Bordeaux 1, Bordeaux, France, 1998.
(17) Blangero, M.; Decourt, R.; Carlier, D.; Ceder, G.; Pollet, M.; Doumerc, J.-P.; Darriet, J.; Delmas, C. *Inorg. Chem.* **2005**, *44*, 9299–9304.
(18) Ménétrier, M.; Carlier, D.; Blangero, M.; Delmas, C. *Electrochem. Solid-State Lett.* **2008**, *11*, 179.
(19) Huang, Q.; Foo, M. L.; Pascal, R. A.; Lynn, J. W.; Toby, B. H.; Tao He, H. W.; Cava, R. J. *Phys. Rev. B* **2004**, *70*, 184110.
(20) Rodriguez-Carvajal, J. *Physica B* **1993**, *192*, 55.
(21) *The International Union of Crystallography, International tables for crystallography, Volume C: Mathematical, Physical and Chemical Tables*; Wilson, A. J. C., Ed.; Kluwer Academic Publishers: London, 1995.
(22) Laplume, J. *L'onde électrique* **1955**, *335*, 113.
(23) Dordor, P.; Marquestaut, E.; Villeneuve, G. *Rev. Phys. Appl.* **1980**, *15*, 1607.
(24) Delmas, C.; Braconnier, J. J.; Fouassier, C.; Hagenmuller, P. *Solid State Ionics* **1981**, *3/4*, 165.

Table 1. Alkali Content from ICP-AES and Average Cobalt Oxidation State from Iodometric Titration

	nominal composition			ICP-AES				iodometric titration (±0.1)
phase	wt % A	wt % Co	x	wt % A	wt % Co	x (±0.01)		Co oxidation state
Li_xCoO_2	4.38	61.97	0.60	4.21	58.57	0.61	3.39	3.35
Na_xCoO_2	13.17	56.27	0.60	14.01	57.92	0.62	3.38	3.2
K_xCoO_2	20.51	51.52	0.60	20.39	50.32	0.61	3.39	3.32

instance, Bañobre-López et al.[25] have reported an increase of the oxygen vacancy content upon sodium deintercalation. They have also noticed a sodium-rate-independent average oxidation state of 3.45 for $x < 0.45$. However, the presence of oxygen vacancies is still debated[26] and some neutron diffraction studies exclude it, even in the highly deintercalated $Na_{0.38}CoO_2$.[27,28]

Structure Determination. All the structures are described with a random distribution of the alkali atoms. The phases can be refined assuming O3, P′3, and P2 structure types for the lithium, sodium, and potassium cobalt double oxides, respectively.

The experimental and refined XRD patterns of O3−$Li_{0.61}CoO_2$ are shown in Figure 2, and the resulting parameters are compiled in Table 2. These results are close to the ones reported by Levasseur.[29] The cobalt−oxygen distance is 1.896 Å. The structure is depicted in Figure 3.

A preliminary observation of the XRD pattern of P′3−$Na_{0.62}CoO_2$ reveals a doubling of several peaks which is characteristic of a lowering in symmetry. With the exception of low intensity peaks between 30 and 45° (Figure 4, inset), the diffractogram can be indexed in the monoclinic system with the space group $C2/m$.[30] The value of the monoclinic angle β (106.069(6)°) is very close to that of the corresponding pseudohexagonal cell (106.549°) and the value of the $a/\sqrt{3}b$ (1.001) ratio is close to unity; this indicates that the distortion is very small. Such a distortion and the observation of the additional peaks between 30 and 45° could result from an in-plane sodium-vacancy ordering.[31] However, we were not successful in identifying this ordering, and the refinement we propose only represents the average disordered structure.

The results of our Rietveld refinement are given in Table 3, and the structure is schematically depicted in Figure 5. The deformation of the CoO_2 layer leads to the loss of the local D_{3d} symmetry. The sodium ion occupies a prismatic site A_{ef}, sharing three edges and one face with the surrounding CoO_6 octahedra. The sodium ion is

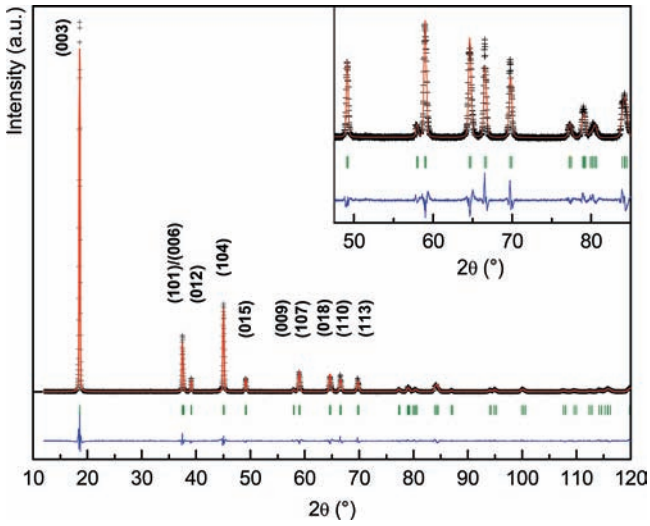

Figure 2. Experimental (crosses) and simulated (solid line) XRD patterns of O3−$Li_{0.61}CoO_2$. (λ: $K\alpha_{Cu}$).

largely shifted from the center of the prism in the three directions, and the Na−O distances vary from 2.223 Å to 2.633 Å. These distances also change depending whether the surrounding CoO_6 octahedra share their face or their edges with the NaO_6 prism. The average Na−O_f distance is longer than the average Na−O_e distance (Figure 5a). The shift in the z direction can be attributed to the fact that the Coulomb interaction is higher through a shared face (shorter Na−Co distance) than through shared edges (longer Na−Co distance).

The in-plane shift can be explained with the Na^+−Na^+ Coulomb repulsion. When a specific site is occupied, the distance to its first possible nearest neighbor is too short (~1.6 Å) as compared to its size (1.02 Å) to allow a simultaneous occupation of sites. The resulting atom distribution then minimizes the electrostatic repulsion between the alkali ions.

The XRD pattern of the P2−$K_{0.61}CoO_2$ phase can be indexed in the hexagonal system (space group $P6_3/mmc$, a = 2.843(2) Å and c = 12.350(1) Å) (Figure 6). The low intensity peaks nearby 35° are unidentified and could be due either to the presence of an impurity or to long-range ordering. Here also, the refinement we propose only represents the average disordered structure. The results of the Rietveld refinement are given in Table 4. The CoO_2 layer packing is of P2-type, and the Co−O distance is 1.902(4) Å. The potassium ions share two prismatic sites, K_f and K_e, with a ratio higher than 1:3. The argument used to explain the in-plane shift of the sodium in P′3−$Na_{0.62}CoO_2$ still applies to the potassium phase: the neighboring site distance (~1.6 Å) is too short as compared to the size of K^+ (1.38 Å) to allow a simultaneous occupation, and the K_e site (6 h) is off-centered (Figure 7) to minimize the electrostatic repulsion.[17]

(25) Bañobre-López, M.; Rivadulla, F.; Caudillo, R.; López-Quintela, M. A.; Rivas, J.; Goodenough, J. B. *Chem. Mater.* **2005**, *17*, 1965.
(26) Kajitani, T.; Begum, S.; Yubuta, K.; Miyazaki, Y.; Igawa, N. Triclinic crystal structure of $[(Bi_{1-x}Co_x)_2(Sr_{1-y}Bi_y)_2O_{4+\delta}]_p[CoO_2]$ with $p \sim 1.05$ and $\delta \sim 0.7$. *Proceedings of the 26th International Conference on Thermoelectrics*, Jeju Island, South Korea, June 3−7, 2007.
(27) Huang, Q.; Foo, M. L.; Pascal, R. A.; Lynn, J. W.; Toby, B. H.; Tao He, H. W.; Cava, R. J. *Phys. Rev. B* **2004**, *70*, 184110.
(28) Viciu, L.; Huang, Q.; Cava, R. J. *Phys. Rev. B* **2006**, *73*, 212107.
(29) Levasseur, S. *Contribution à l'étude des phases Lix(Co,M)O2 en tant que matériau d'électrode positive des batteries Li-ion. Effets combinés de la surstœchiométrie en lithium et de la substitution* (M = *Ni, Mg*). Ph.D. Thesis, Université de Bordeaux 1, Bordeaux, France, 2001.
(30) Ono, Y.; Ishikawa, R.; Miyazaki, Y.; Ishii, Y.; Morii, Y.; Kajitani, T. *J. Solid State Chem.* **2002**, *166*, 177.
(31) Blangero, M.; Carlier, D.; Pollet, M.; Darriet, J.; Delmas, C.; Doumerc, J.-P. *Phys. Rev. B* **2008**, *77*, 184116.

Table 2. Structure Refinement for the O3−$Li_{0.61}CoO_2$ Phase

cell parameters						
space group: $R3\overline{m}$ (Z = 3) a = 2.809(2) Å − c = 14.319(1) Å						
atomic positions						
atom	site	x	y	z	B_{iso} (Å^2)	S.O.F.
Li	3b	0	0	1/2	2.6(5)	0.61
Co	3a	0	0	0	0.16(2)	1
O	6c	0	0	0.2648(2)	0.23(6)	1
conventional reliability factors						
cR_{wp} = 19.0% − cR_{exp} = 10.0% − χ^2 = 3.61 − R_{Bragg} = 4.43%						

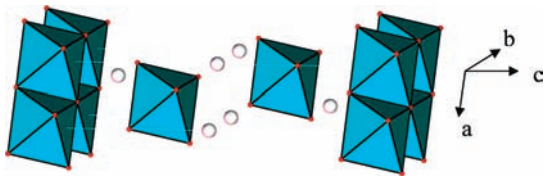

Figure 3. Representation of the O3−$Li_{0.61}CoO_2$ phase.

The main structural characteristics of the A_xCoO_2 ($x \sim 0.6$) compounds are listed in Table 5, and several effects of the alkali change can be highlighted. (i) The alkali-oxygen distances are in agreement with the data provided by Shannon.[32] (ii) The AO_2 interslab thickness increases with the alkali ionic radius resulting in an increase in the 2D character from lithium to potassium cobalt double oxides. (iii) The angle θ between the z-axis and Co−O bond direction. This angle quantifies the amplitude of the D_{3d} distortion. In hexagonal symmetry, it is given by $\theta = \arcsin(d_{Co-Co} = \sqrt{3} \times d_{Co-O})$. For a regular octahedron (O_h), $d_{Co-Co} = \sqrt{2} \times d_{Co-O}$ and $\theta_h = \arcsin(\sqrt{2}/\sqrt{3}) \approx 54.74°$. Here, all the CoO_6 octahedra are compressed leading to $\theta > \theta_h$. When the alkali content is fixed, the cobalt−oxygen distance remains close to 1.90 Å, in agreement with the ionic radius sum. On the other hand, mainly because of the alkali size effect, the Co−Co distance increases significantly from Li to K leading to the increase of θ. For the lithium and potassium phase which have a hexagonal symmetry, the simultaneous increase in θ and very small decrease in the CoO_2 layer thickness can be explained by a O−O distance that remains nearly unchanged for CoO_6 octahedron common edges (2.547 Å for O3−$Li_{0.61}CoO_2$ and 2.528 Å for P2−$K_{0.61}CoO_2$). Actually, this O−O distance cannot decrease below the contact distance, and similar arguments have been used to explain the low change in this distance in delafossites when the trivalent ion is changed.[33,34] (iv) The CoO_2 layer thickness, as the mean Co−O distance, does not change monotonically on changing the alkali from lithium to potassium. There is a decrease from the sodium to the potassium phase as expected from an antagonist bond scheme where the higher ionicity of the potassium reinforces the covalent character of the Co−O bond. In the case of the lithium phase this trend is broken and the CoO_2 layer thickness is lower but close to the one of the sodium compound; the Co−O distance decreases as well in the lithium compound and is the lowest among the 3 phases. This change in the CoO_2 layer thickness is believed to be due to the complex interplay between the increase of covalence of the Co−O bond with the electropositive character of the alkali, the cell expansion due to size effect, and the change in the oxygen environment of the alkali (octahedron for the lithium and prisms for the sodium and the potassium), and further the alkali environment of the cobalt that changes dramatically in the different compounds (only edge sharing with lithium ions but both edge and face sharing in different proportions with sodium and potassium ions). Obviously, the result for these cross effects cannot be simply anticipated. One may note that this last point has been the subject of several theoretical reports pointing out that the sodium potential favors the electronic correlations.[35,36] The existence of two different crystal sites Na_e/Na_f and of vacancies randomly distributed in the sodium layer creates a non uniform electrostatic

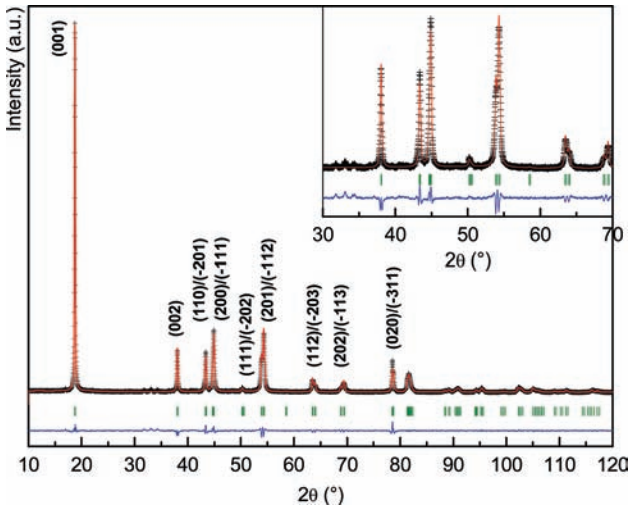

Figure 4. Experimental (crosses) and simulated (solid line) XRD patterns of P′3−$Na_{0.62}CoO_2$. (λ: Kα_{Co}).

(32) Shannon, R. D. *Acta. Crystallogr. A* **1979**, *32*, 751.
(33) Isawa, K.; Yaegashi, Y.; Komatsu, M.; Nagano, M.; Sudo, S.; Karppinen, M.; Yamauchi, H. *Phys. Rev. B* **1997**, *56*, 3457.
(34) Tate, J.; Jayaray, M. K.; Draeseke, A. D.; Ulbrich, T.; Sleight, A. W.; Vanaja, K. A.; Nagarajan, R.; Wager, J. F.; Hoffman, R. L. *Thin Solid Films* **2002**, *411*, 119.
(35) Zhang, P.; Capaz, R. B.; Cohen, M. L.; Louie, S. G. *Phys. Rev. B* **2005**, *71*, 153102.
(36) Merino, J.; Powell, B. J.; McKenzie, R. H. *Phys. Rev. B* **2006**, *73*, 235107.

Table 3. Structure Refinement for the P′3−$Na_{0.62}CoO_2$ Phase

cell parameters						
space group: $C2/m$ ($Z = 2$) $a = 4.900(1)$ Å − $b = 2.826(1)$ Å − $c = 5.716(1)$ Å − $\beta = 106.069(6)°$						
atomic positions						
atom	site	x	y	z	B_{iso} (Å^2)	S.O.F.
Na	8j	0.820(2)	0.098(5)	0.492(1)	0.6(1)	0.155
Co	2a	0	0	0	0.71(3)	1
O	4i	0.3892(6)	0	0.1791(4)	0.60(5)	1
conventional reliability factors						
$cR_{wp} = 11.1\% - cR_{exp} = 6.42\% - \chi^2 = 2.99 - R_{Bragg} = 2.71\%$						

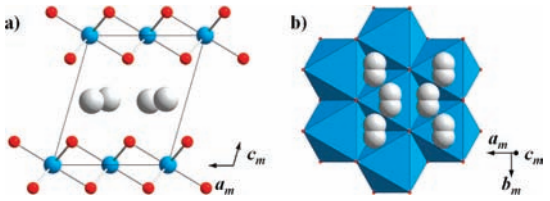

Figure 5. (a) Representation of the monoclinic cell of P′3−$Na_{0.62}CoO_2$ along the b_m axis, and (b) projection in the (ab) plane showing the off-center position of sodium ($z \sim 0.5$).

potential in the CoO_2 sheets that could contribute to charge localization.[37] Marianetti et al.[38] have proposed a Hamiltonian accounting for this potential and have evidenced that the conducting sheets are much more perturbed at $x = 0.7$ than at $x = 0.3$ and that the charge localization is greater for $x > 0.5$; they were also able to simulate the Curie−Weiss behavior for $x = 0.7$ and the Pauli one for $x = 0.3$. The position of Na_f in the P2 phase is of particular interest: this site is surrounded along the z axis by two cobalt ions, and its occupation is energetically more costly than the one of Na_e, but it is compensated by the global minimization of the coulomb interaction between the sodium cations.[17] As already mentioned, with this coordination, the a_{1g} orbitals of the cobalt ($d_{z^2-r^2}$ along the 3-fold axis) are directly pointing toward the Na_f sites that can favor electron localization at the center of this dumbbell to minimize the coulomb repulsion. Several ^{59}Co NMR studies[39−42] support this idea with the observation of several cobalt sites for $x \sim 0.7$ while only one is observed for $x \sim 0.3$. The fact that only one site is detected for $x \sim 0.3$ strengthens the idea that the sodium potential is screened by a higher charge carrier concentration and is not anymore a perturbation for CoO_2 layer.[43] Recent studies[44−47] report on the cationic ordering in the interslab and clusters configurations of Na_f/Na_e for $x > 0.7$, suggesting the simultaneous presence of localized spins and itinerant charge carriers.

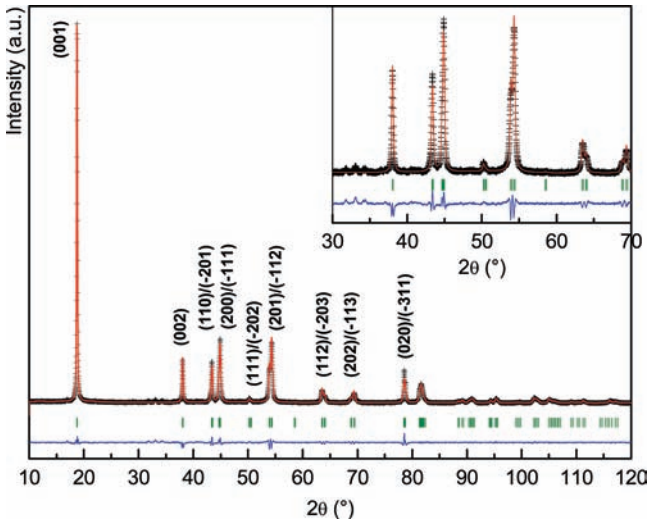

Figure 6. Experimental (crosses) and simulated (solid line) XRD patterns of P2−$K_{0.61}CoO_2$. (λ: $K\alpha_{Co}$).

Transport Properties. As the compactness of our cold-pressed pellets is close to 70% only, the measured values of the electrical resistivity is probably much higher than the intrinsic value. However, we still assume that the temperature dependence is meaningful. The temperature dependence from 4 to 300 K of the electrical resistivity for the polycrystalline samples is shown in Figure 8. All three materials have a metallic behavior ($\partial\rho/\partial T > 0$).

The linear variation of the resistivity for O3−$Li_{0.61}CoO_2$ and P′3−$Na_{0.62}CoO_2$, unlike the one for a conventional metal, suggests no change in the carrier diffusion mechanism. This behavior has been attributed to strong

(37) Gao, M.; Zhou, S.; Wang, Z. *Phys. Rev. B* **2007**, *76*, 180402.
(38) Marianetti, C. A.; Kotliar, G. *Phys. Rev. Lett.* **2007**, *98*, 176405.
(39) Mukhamedshin, I. R.; Alloul, H.; Collin, G.; Blanchard, N. *Phys. Rev. Lett.* **2004**, *93*, 167601.
(40) de Vaulx, C. *Etude par résonance magnétique nucléaire de cobaltates NaxCoO2*. Ph.D. Thesis, Université Joseph Fourier de Grenoble I, Grenoble, France, 2007.
(41) Ning, F. L.; Imai, T.; Statt, B. W.; Chou, F. C. *Phys. Rev. Lett.* **2004**, *93*, 237201.
(42) Mukhamedshin, I.R.; Alloul, H.; Collin, G.; Blanchard, N.; Influence of Charge order on the Magnetic Properties of NaxCoO2 for $x > 0.65$, arXiv:0703.561v1 [cond-mat.str-el], (**2007**)
(43) Mukhamedshin, I. R.; Alloul, H.; Collin, G.; Blanchard, N. *Phys. Rev. Lett.* **2005**, *94*, 247602.
(44) Roger, M.; Morris, D. J. P.; Tennant, D. A.; Gutmann, M. J.; Goff, J. P.; Hoffmann, J. U.; Feyerherm, R.; Dudzik, E.; Prabhakaran, D.; Boothroyd, A. T.; Shannon, N.; Lake, B.; Deen, P. P. *Nature* **2007**, *445*, 631.
(45) Chou, F.C.; , Chu, M. W.; , Shu, G. J.; Huang, F. T.; Pai, W. W.; Sheu, H. S.; Imai, T.; Ning, F. L.; Lee, P. A. Sodium vacancy ordering and the co existence of localized spins and itinerant charges in NaxCoO2, *arXiv*:0709.0085 [cond-mat.str-el], **2007**.
(46) Julien, M. H.; de Vaulx, C.; Mayaffre, H.; Berthier, C.; Horvatić, M.; Simonet, V.; Wooldridge, J.; Balakrishnan, G.; Lees, M. R.; Chen, D. P.; Lin, C. T.; Lejay, P. Electronic texture of the thermoelectric oxide Na0.75-CoO2. *arXiv*:0801.4095 [cond-mat.str-el], (**2008**.
(47) Balicas, L.; Jo, Y. J.; Shu, G. J.; Chou, F. C.; Lee, P. A. *Phys. Rev. Lett.* **2008**, *100*, 126405.

Table 4. Structure Refinement for the P2−$K_{0.61}CoO_2$ Phase

cell parameters						
space group: $P6_3/mmc$ (Z = 2) a = 2.843(2) Å − c = 12.350(1) Å						
atomic positions						
atom	site	x	y	z	B_{iso} (Å ^{2})	S.O.F.
K_e	6 h	0.522(3)	0.261(2)	1/4	2.4(5)	0.138(1)
K_f	2b	0	0	1/4	1.1(7)	0.197(1)
Co	2a	0	0	0	0.9(1)	1
O	4f	$^1/_3$	$^2/_3$	0.0779(5)	0.7(2)	1
conventional reliability factors						
cR_{wp} = 17.1% − cR_{exp} = 10.4% − χ^2 = 2.73 − R_{Bragg} = 4.57%						

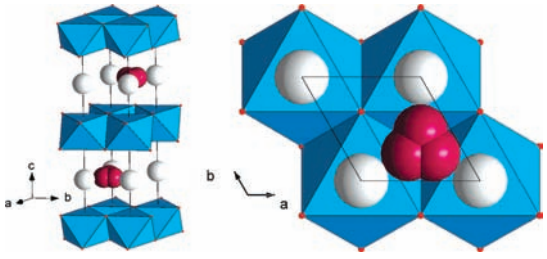

Figure 7. (Left) Representation of the P2−$K_{0.61}CoO_2$ phase and (Right) Representation of the manifold potassium sites: K_e (2b in violet) and K_f (6 h in white).

Table 5. Interatomic Distances in A_xCoO_2 (A = Li, Na, K; $x \sim 0.6$) and θ Angle between the 3-Axis [a] and the Pseudo-4-Axis[b]

A_xCoO_2	O3−$Li_{0.61}$-CoO_2	P′3−$Na_{0.62}$-CoO_2	P2−$K_{0.61}$-CoO_2
CoO_2 layer thickness (Å)	1.963	1.967	1.923
AO_2 interslab thickness (Å)	2.810	3.526	4.252
average d_{A-O} (Å)	2.146(2)	2.416(9)	2.698(6)
average d_{Co-Co} (Å)	2.809(2)	2.828(1)	2.843(2)
average d_{Co-O} (Å)	1.896(1)	1.905(3)	1.902(4)
θ	58.80°	59.09°	59.65°

[a] Pseudo-axis in the case of P′3−$Na_{0.62}CoO_2$). [b] Co−O bond axis.

electron correlations.[48,49] On the opposite, the potassium cobalt double oxide exhibits a residual component at low temperature and tends to the classical behavior of electron diffusion by the phonons when the temperature increases.[50] Note that the resistivity of P2−$K_{0.61}CoO_2$ is higher than that of the ordered compound P2−$K_4Co_7O_{14}$ from 10 times at 4 K to 2 times at room temperature (RT).[17] As the compactness of the sample is the same, this result could be ascribed to the disordered distribution of the potassium that induces random variation of the Madelung energy leading to the decrease of the elastic

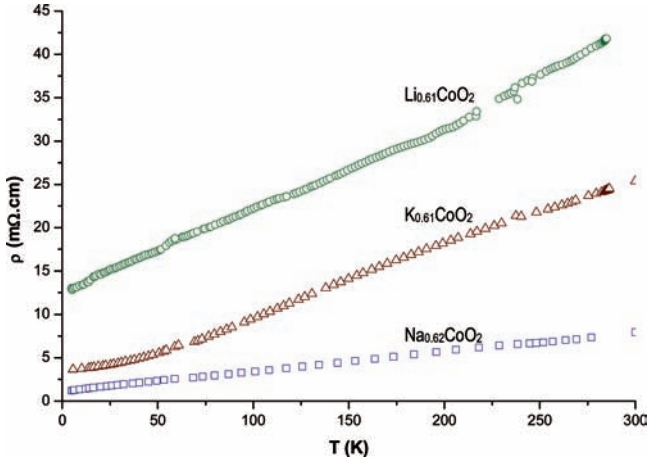

Figure 8. Temperature dependence of the electric resistivity for O3−$Li_{0.61}CoO_2$ (green circles), P′3−$Na_{0.62}CoO_2$ (blue squares), and P2−$K_{0.61}CoO_2$ (red triangles).

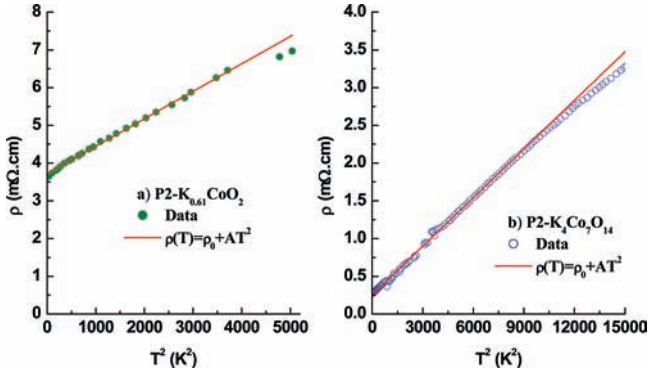

Figure 9. Variation of the electrical resistivity vs T^2 for (a) P2−$K_{0.61}CoO_2$ and (b) P2−$K_4Co_7O_{14}$.[17]

carrier diffusion length. At low temperature, the data follow a T^2 law, typical of the electron−electron scattering in a Fermi liquid: $\rho(T) = \rho_0 + AT^2$; ρ_0 depends on extrinsic parameters like grain boundaries, impurities, structural defects, and so forth, and A is characteristic of the electron interaction. Figure 9 shows the resistivity versus T^2 plots for both the disordered and the ordered potassium phases. The linear domain holds up to 60 K in the case of the disordered phase with ρ_0 = 3.72 mΩ cm and $A = 7.26 \times 10^{-4}$ mΩ cm/K^2 while it ends at 100 K for

(48) Rivadulla, F.; Zhou, J. S.; Goodenough, J. B. *Phys. Rev. B* **2003**, *68*, 75108.
(49) Wang, Y.; Rogado, N. S.; Cava, R. J.; Ong, N. P. *Nature* **2003**, *432*, 425.
(50) Nakamura, S.; Ohtake, J.; Yonezawa, N.; Iida, S. *J. Phys. Soc. Jpn.* **1996**, *65*, 358.

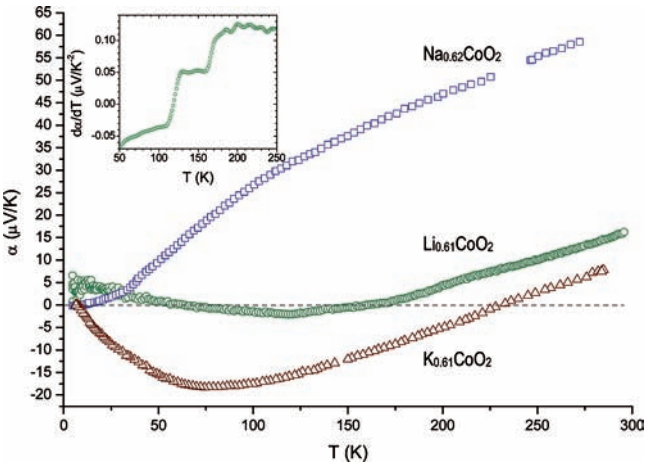

Figure 10. Temperature dependence of the thermopower for O3−$Li_{0.61}CoO_2$ (green circles), P′3−$Na_{0.62}CoO_2$ (blue squares), and P2−$K_{0.61}CoO_2$ (red triangles). Inset: first derivative of the thermopower for O3−$Li_{0.61}CoO_2$.

the ordered cobalt double oxide with $\rho_0 = 0.254$ mΩ cm and $A = 2.15 \times 10^{-4}$ mΩ cm/K^2.

Keeping in mind that the values for A might be overestimated because of the low compactness of our samples, we can still note that the calculated values for A are much larger than for metals such as Al and Mo ($A_{Al} = 2.8 \times 10^{-10}$ mΩ cm/K^2;[51] $A_{Mo} = 1.26 \times 10^{-9}$ mΩ cm/K^2[52]) and they suggest a strong electron correlation effect.[53] In addition, they are close to the ones determined for single crystals of $Na_{0.7}CoO_2$ ($A_{(ab)} = 9.6 \times 10^{-4}$ mΩ cm/K^2 below 2 K[54]) and $Ca_3Co_4O_9$ ($A = 3.6 \times 10^{-5}$ mΩ cm/K^2 [55,56]).

The thermopower temperature dependence strongly changes with the alkali element (Figure 10). It is positive, and it continuously increases for the sodium phase whereas its sign changes for the lithium and potassium compounds. Above 90 K, the thermopower increases monotonically in the case of the potassium phase. On the other hand, two linear regimes are visible for the lithium compounds as shown in the inset of Figure 10 with the plot of the first derivative. A transition regime is present from near 160 to 200 K.

The values for the thermopower at 280 K and the slopes in the high (250 K < T < 300 K) and low temperature (4 K < T < 25 K) regions are given in Table 6.

All the three compounds have similar slopes at high temperature, significantly higher (~10 times) than the thermopower predicted for a free electron gas. This difference can be ascribed to the reinforcement of the charge carriers effective mass, the 3d bands being generally quite narrow in transition metal oxides.[57] The result for O3−$Li_{0.61}CoO_2$ obtained in this work differs from the one of Ménétrier et al.[58] who obtained a quasi-linear dependence of the thermopower up to 300 K and a slightly larger slope (0.169 μV/K^2). The difference is probably due to our synthesis method which avoids substitution of lithium for cobalt in the CoO_2 layers while a small difference in the alkali content cannot be totally discarded.

Table 6. Values of the Thermopower at 280 K and Slopes at High and Low Temperature[a]

phase	α (280 K) (μV/K)	dα/dT (μV/K^2)	R^2 (%)	dα/dT (250−300 K) (μV/K^2)	R^2 (%)
O3−$Li_{0.61}CoO_2$	16.4			0.133	97.75
P′3−$Na_{0.62}CoO_2$	59.0	0.110	97.45	0.165	99.91
P2−$K_{0.61}CoO_2$	8.0	−0.375	99.51	0.151	99.91

[a] The slope at low temperature is given for T < 25 K for the sodium phase and for T < 50 K for the potassium phase (R^2: reliability factor).

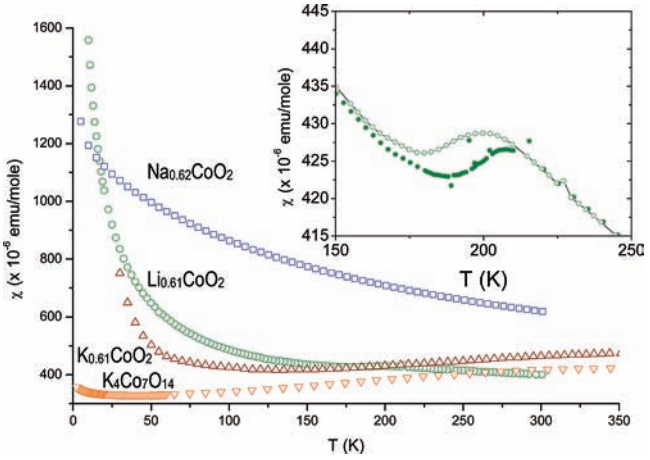

Figure 11. Evolution of the magnetic susceptibility vs temperature for O3−$Li_{0.61}CoO_2$ (green circles), P′3−$Na_{0.62}CoO_2$ (blue squares), P2−$K_{0.61}CoO_2$ (red triangles), and P2−$K_4Co_7O_{14}$ (orange triangles) [Blangero et al. *Inorg. Chem.* **2005**, *44*, 9299−9304]. The inset shows an enlargement of the zero-field-cooled (full circles) and filled-cooled (empty circles) data for O3−$Li_{0.61}CoO_2$.

Magnetic Properties. The linearity of the magnetization versus the magnetic field has been checked for all samples and, as shown in Figure 11, the resulting magnetic susceptibility considerably changes with the nature of the alkali. All samples have a paramagnetic behavior; however, it looks Curie−Weiss-like for the lithium and sodium compounds while it is Pauli-like above 60 K in the case of the potassium phase. The lithium cobalt double oxide displays a magnetic hysteresis between 160 and 210 K (Figure 11, inset) that will be discussed later.

Above 60 K, the P2−$K_{0.61}CoO_2$ phase exhibits, as the corresponding ordered compound P2−$K_4Co_7O_{14}$,[17] a nearly temperature independent susceptibility (Figure 11). The possible contributions are a core electron diamagnetism χ_{dia}, a second order orbital paramagnetism χ_{vv}, and a

(51) Ribot, J.H.J.M; Bass, J.; Kempen, H.; Vucht, R. J. M.; Wider, P. *Phys. Rev. B* **1981**, *23*, 532.
(52) Ruthruff, T. L.; Grenier, C. G.; Goodrich, R. G. *Phys. Rev. B* **1978**, *17*, 3070.
(53) Georges, A.; Kotliar, G.; Krauth, W.; Rozenberg, M. *Rev. Mod. Phys.* **1996**, *68*, 13.
(54) Li, S.Y.; Taillefer, L.; Hawthorn, D. G.; Tanatar, M. A.; Paglione, J.; Sutherland, M.; Hill, R. W.; Wang, C. H.; Chen, X. H. *Phys. Rev. Lett.* **2004**, *93*, 56401.
(55) Limelette, P.; Hardy, V.; Auban-Senzier, P.; Jérome, D.; Flahaut, D.; Hébert, S.; Frésard, R.; Simon, C.; Noudem, J.; Maignan, A. *Phys. Rev. B* **2005**, *71*, 233108.
(56) Eng, H. W.; Limelette, P.; Prellier, W.; Simon, C.; Frésard, R. *Phys. Rev. B* **2006**, *73*, 033403.
(57) Goodenough, J. B. *Prog. Solid State Chem.* **1971**, *5*, 145.
(58) Ménétrier, M.; Saadoune, I.; Levasseur, S.; Delmas, C. *J. Mater. Chem.* **1999**, *9*, 1135.

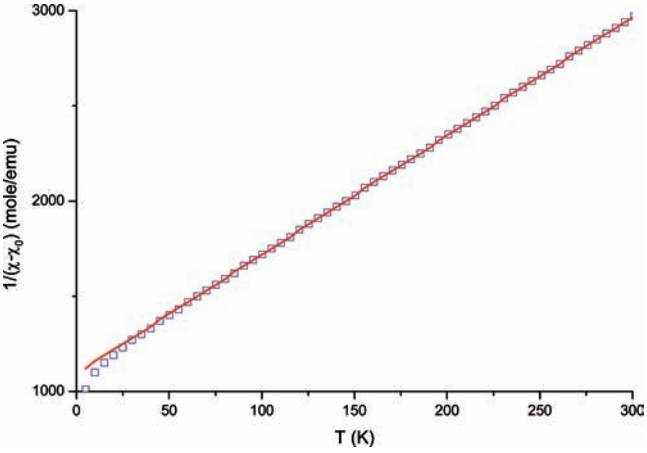

Figure 12. Evolution of the inverse of the magnetization vs temperature for P′3−$Na_{0.62}CoO_2$ (blue squares). The line is the fit to the Curie−Weiss law.

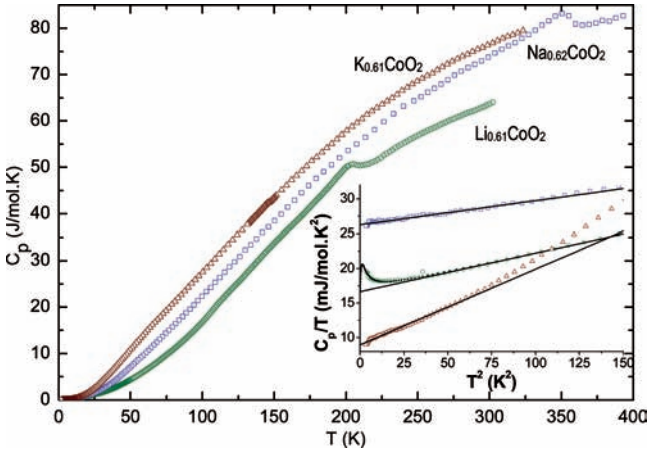

Figure 13. Specific heat vs temperature for O3−$Li_{0.61}CoO_2$ (green circles), P′3−$Na_{0.62}CoO_2$ (blue squares), and P2−$K_{0.61}CoO_2$ (red triangles). Inset: plots of C_p/T vs T^2; solid lines are the fits to the Debye model, and the dot-line (O3−$Li_{0.61}CoO_2$) includes a Schottky contribution.

contribution of the itinerant carriers χ_e. χ_{dia} can be estimated from the international tables to be -41×10^{-6} emu/mol. χ_{vv} because of LS-Co^{3+} generally ranges from 150×10^{-6} to 250×10^{-6} emu/Co^{3+}-mole;[59,60] the observed susceptibility ranges from 415×10^{-6} to 460×10^{-6} emu/mol, and χ_e is estimated to range from 300 to 410×10^{-6} emu/mol. The μ^+SR (Muons Spin Relaxation) experiments carried out on both the ordered and disordered phases confirm the Pauli-type character down to 1.8 K.[61] However, the P2−$K_{0.61}CoO_2$ phase displays a fast increase in magnetization below 60 K and a divergence of the ZFC and FC curves at about 30 K (not shown) suggesting the existence of localized moments. The μ^+SR study indeed reveals a spin-glass behavior with a fast decrease in $A_0P_{zf}(t)$ between $0 < t < 1$ μs that is characteristic of localized and disordered moments. This suggests that P2−$K_{0.61}CoO_2$ is at the border of the Pauli/Curie−Weiss transition ($x_c \sim 0.6$) as it was proposed for the P2−Na_xCoO_2 system.[62] The large value of χ_e, about 10 times higher than that of the free electron gas, can be explained by electron correlations as expected from a Fermi liquid.

Figure 12 shows the fit of the data to a Curie−Weiss law for P′3−$Na_{0.62}CoO_2$: $\chi = \chi_{dia} + \chi_0 + C/(T - \theta_p)$, χ_0 a temperature independent paramagnetism term (TIP), C the Curie constant, and θ_p the Weiss temperature. The data for this sodium phase are perfectly fitted above 20 K with $\chi_0 = 344.10^{-6}$ emu/mol, $C = 0.16$, and $\theta_p = -174$ K. Assuming low spin states (LS) for both Co^{3+} ($S = 0$) and Co^{4+} ($S = 1/2$), the amount of Co^{4+} is estimated to be 0.43; neglecting the oxygen deficiency suggested by iodometric titration, this leads to a sodium content of 0.57 that is quite close to the nominal composition and the value obtained from ICP-AES (Table 1). The large value of $|\theta_p|$ is more complex to analyze: it could result either from dominant antiferromagnetic interactions or, as suggested from the transport measurements, from strong electron correlations. This Curie−Weiss behavior of P′3−$Na_{0.62}CoO_2$ agrees with the magnetic phase diagram of the system P2−Na_xCoO_2 for $x > 0.5$.

The magnetic behavior of O3−$Li_{0.61}CoO_2$ is blurred with traces of cobalt oxide[63] not seen by XRD, and the increase in magnetization upon decreasing temperature might be partly due to the presence of this impurity. A recent study of the Li_xCoO_2 system[64] indeed points out that the behavior is expected to be Pauli-like for $x < 1$ with intermediate or weakly coupled electrons. Sugiyama et al.[65,66] have also recently studied the O3−Li_xCoO_2 with $0.7 \leq x \leq 1$. They have observed a feature at 170 K that they attribute to a spin transition of Co^{4+}. They have also proposed a similar transition for the misfit compound $[Ca_2CoO_3]_{0.62}[CoO_2]$.[67] For O3−$Li_{0.7}CoO_2$, assuming high spin (HS) states, they report a Curie−Weiss behavior with a surprisingly large $|\theta_p|$ value ($\theta_p \sim -800$ K). Such a large $|\theta_p|$ value has never been reported in another cobalt oxides. Very strong antiferromagnetic interactions are observed in some perovskites with strong 180°-super-exchange like in the Mott-Hubbard insulator La_2CuO_4. Such apparent Curie−Weiss behaviors with extremely large $|\theta_p|$ values are also found in highly correlated metals. Generally speaking, the HS state in Co^{3+} is quite rare except in the case of strong axial distortion along the 4-axis;[68] in the case of a prismatic environment, it was reported for the 1D compound $Ca_3Co_2O_6$.[69] The HS state is even less expected for Co^{4+} since its smaller size is inducing a stronger crystal-field. Note also that the

(59) Ballhausen, J. *Introduction to Ligand Field Theory*; McGraw-Hill: New York, 1962.
(60) Mabbs, F. E.; Machin, D. J. *Magnetism and Transition Metal Complexes*; Chapman Hall: London, 1973.
(61) Sugiyama, J.; Ikedo, Y.; Russo, P. L.; Nozaki, H.; Mukai, K.; Andreica, D.; Amato, A.; Blangero, M.; Delmas, C. *Phys. Rev. B* **2007**, *76*, 104412.
(62) Yoshizumi, D.; Muraoka, Y.; Okamoto, Y.; Kiuchi, Y.; Yamaura, J.; Mochizuki, M.; Ogata, M.; Hiroi, Z. *J. Phys. Soc. Jpn.* **2007**, *76*, 63705.
(63) Artemenko, A.; Ménétrier, M.; Pollet, M.; Delmas, C. *J. Appl. Phys.* **2009**, in press.
(64) Mukai, K.; Ikedo, Y.; Nozaki, H.; Sugiyama, J.; Nishiyama, K.; Andreica, D.; Amato, A.; Russo, P. L.; Ansaldo, E. J.; Brewer, J. H.; Chow, K. H.; Ariyoshi, K.; Ohzuku, T. *Phys. Rev. Lett.* **2007**, *99*, 087601.
(65) Sugiyama, J.; Nozaki, H.; Brewer, J. H.; Ansaldo, E. J.; Morris, G. D.; Delmas, C. *Phys. Rev. B* **2005**, *72*, 144424.
(66) Sugiyama, J.; Nozaki, H.; Brewer, J. H.; Ansaldo, E. J.; Morris, G. D.; Delmas, C. *Physica B* **2006**, *374 375*, 148.
(67) Sugiyama, J.; Brewer, J. H.; Ansaldo, E. J.; Itahara, H.; Dohmae, K.; Seno, Y.; Xia, C.; Tani, T. *Phys. Rev. B* **2003**, *68*, 134423.
(68) Doumerc, J. P.; Coutanceau, M.; Fournès, L.; Grenier, J. C.; Pouchard, M.; Wattiaux, A. *C.R. Acad. Sci. Paris Série IIc* **1999**, *2*, 637.
(69) Aasland, S.; Fjellvåg, H.; Hauback, B. *Solid State Commun.* **1997**, *101*, 187.

Table 7. Values of the Fit Parameters γ and θ_D for the Debye Model Approximation $C_p(T)/T = \gamma + \beta T^2$ [a]

phase	model	γ (J/mol K^2)	β (J/mol K^4)	θ_D (K)	c_0 (J/mol K^2)	T_0 (K)	R^2 (%)
O3−$Li_{0.61}CoO_2$	Debye	16.6×10^{-3}	5.56×10^{-5}	501			99.96
O3−$Li_{0.61}CoO_2$	Debye + Schottky	16.7×10^{-3}	5.48×10^{-5}	504	11.75×10^{-3}	3.78	99.72
P′3−$Na_{0.62}CoO_2$	Debye	26.1×10^{-3}	3.92×10^{-5}	562			97.60
P2−$K_{0.61}CoO_2$	Debye	9.0×10^{-3}	10.9×10^{-5}	401			99.29
P2−$K_4Co_7O_{14}$	Debye	8.8×10^{-3}	10.7×10^{-5}	404			97.60

[a] The parameters of the Schottky anomaly for O3−$Li_{0.61}CoO_2$ are given. In addition, the results for the ordered P2−$K_4Co_7O_{14}$ phase are provided for comparison [Blangero et al. *Inorg. Chem.* **2005**, *44*, 9299−9304] (R^2: reliability factor).

trigonal distortion (θ in Table 5) decreases with decreasing size of the alkali atom, and, thus, among the three compounds O3−$Li_{0.61}CoO_2$ should have the smallest probability of containing HS cobalt.

Specific Heat Measurements. The results of specific heat measurements are plotted in Figure 13. The asymptotic limit of Dulong and Petit[70] ($3 \times 3.6 \times R \approx 90$ J/mol K) is fast reached in the case of the sodium and potassium cobalt double oxides while the convergence is slower for the lithium phase. The data display anomalies at about 200 K for O3−$Li_{0.61}CoO_2$ and about 350 K for P′3−$Na_{0.62}CoO_2$ that will be discussed later. In the lithium case, it seems related to the different regimes already observed with the thermopower and magnetic measurements.

The Sommerfeld coefficient, γ, has been evaluated using the Debye model approximation between 1.8 and 10 K: $C_p(T)/T = \gamma + \beta T^2$. In this expression, β is characteristic of the lattice contribution at low temperature and depends on n_D (~ 3.6) the number of Debye-type vibrators and θ_D the Debye temperature: $\beta = 12\pi^4 R n_D / 5\theta_D^3$. The plots for $C_p/T(T^2)$ are shown in the inset of Figure 13, and the fit parameters are given in Table 7. Note that in the case of the lithium phase, C_p/T fast increases for $T^2 < 12$ K^2. This behavior is characteristic of a Schottky contribution C_S ($C_s(T)/T = c_0 \cdot [T_0^2 \exp(T_0/T)]/[T^3 (\exp(T_0/T) + 1)^2]$) the origin of which is still undetermined;[71,72] however, it is likely to be associated with 2-level excitations between impurities and major phase. Taking into account this last contribution does not lead to significant changes in the values of γ and θ_D. The characteristic temperature of the Schottky anomaly is low (3.78 K), and specific heat measurements at lower temperature would be useful to further interpret this result. The change in θ_D with the alkali is, at first sight, unexpected, and treating equivalently the interslab for all materials, a decrease in θ_D from Li to Na and then K phase is, a priori, expected because of the increase in the molar weight of the cation. This is the case for the two last compounds that actually share a similar structure with a prismatic environment of the alkali. However, the lithium compound with an octahedral environment of the alkali might be seen as the exception for this series of compounds resulting in an intermediate value of θ_D. It can actually be also remarked that the trend for θ_D follows the one for the CoO_2 layer thickness (and average Co−O distance; see Table 5), and we cannot discard any cross effect even though no clear model can be proposed.

As already pointed out, the lithium and sodium compounds display an anomaly in the specific heat data. Such a transition has already been evidenced not only in P′3−$Na_{0.62}CoO_2$ ($T_S \sim 350$ K)[31] but also in P2−$Na_{\sim 0.7}CoO_2$ ($T_S \sim 336$ K),[73] P2−$Na_{0.5}CoO_2$ ($T_S \sim 470$ K),[74] P2−$K_{0.5}CoO_2$ ($T_S \sim 550$ K),[75] P′3−$K_{0.5}CoO_2$[76] ($T_S \sim 525$ K), and in P2−$K_4Co_7O_{14}$ ($T_S \sim 458$ K);[77] it was attributed to the change of alkali mobility in the interslab. It can be noticed that the transition temperature (200, 350, and 458 K for respectively O3−$Li_{0.61}CoO_2$, P′3−$Na_{0.62}CoO_2$, and P2−$K_4Co_7O_{14}$ ($x \sim 0.57$)) linearly varies with the inverse of the alkali ionic radii and mass.[32] Even though this dependence is not easily interpreted, it suggests that the transitions might have a similar origin, that is, in the three cases the freezing of alkali at low temperature.

Discussion

Table 8 summarizes some of the main trends observed in the electronic properties of the materials studied in this work. No clear correlation appears between the alkali nature, the difference in the packing, and the properties; however some conclusions can still be drawn concerning these systems.

Potassium Phase, a Fermi Liquid Behavior. The increase in the effective mass of quasi-particles is mainly observed in parameters such as in χ_{Pauli}, γ, A, and the low temperature slope of the thermopower ($d\alpha/dT$). It follows that all our results converge to the conclusion of weak to intermediate correlations: the electric resistivity of P2−$K_{0.61}CoO_2$ is typical of a metal (Figure 8), and at low temperature, it follows a T^2 law (with a large slope: $A = 7.263 \times 10^{-4}$ mΩ cm/K^2) characteristic of electron−electron scattering as expected for a Fermi liquid; its thermopower remains quite low but the slopes are anyway roughly 10 times higher than the one of the free electron gas (Figure 10); it exhibits a Pauli-like behavior (Figure 11) with a reinforced value of the susceptibility nearly 1 order of magnitude higher than for the electron gas (300 to 410×10^{-6} emu/mol); the Sommerfeld coefficient determined from the specific heat measurements (Figure 13) is slightly enhanced with $\gamma = 9 \times 10^{-3}$ J/mol K^2. Hereafter, we numerically compare the electronic behavior of P2−$K_{0.61}CoO_2$ to the one of the free electron

(70) Petit, A. T.; Dulong, P. L. *Ann. Chim. Phys.* **1819**, *10*, 395.
(71) Ando, Y.; Miyamoto, N.; Segawa, K.; Kawata, T.; Terasaki, I. *Phys. Rev. B* **1999**, *60*, 10580.
(72) Limelette, P.; Hébert, S.; Hardy, V.; Frésard, R.; Simon, C.; Maignan, A. *Phys. Rev. Lett.* **2006**, *97*, 46601.
(73) Wooldridge, J.; McK, D; Paul, G.; Balakrishnan; Lees, M. R. *J. Phys.: Condens. Matter* **2005**, *17*, 707–718.
(74) Yang, H. X.; Nie, C. J.; Shi, Y. G.; Yu, H. C.; Ding, S.; Liu, Y. L.; Wu, D.; Wang, N. L.; Li, J. Q. *Solid State Commun.* **2005**, *134*, 403.
(75) Watanabe, H.; Mori, Y.; Yokoi, M.; Moyoshi, T.; Soda, M.; Yasui, Y.; Kobayashi, Y.; Sato, M.; Igawa, N.; Kakurai, K. *J. Phys. Soc. Jpn.* **2006**, *75*, 34716.
(76) Blangero, M., unpublished.
(77) Blangero, M., unpublished.

Table 8. Electronic Properties of $A_{0.6}CoO_2$ [a]

phase	ρ (LT)	α	χ	γ (J/mol/K^2)	c/Za	packing
$Rb_{0.5}CoO_2$ [c]	metallic		Pauli		2.32	P2
$K_4Co_7O_{14}$ [d]	$\propto T^2$	bad metal	enhanced-Pauli	8.8×10^{-3}	2.18	P2
$K_{0.61}CoO_2$ [b]	$\propto T^2$	bad metal	enhanced-Pauli	9×10^{-3}	2.17	P2
$Na_{0.31}CoO_2$ [e−f]		bad metal	enhanced-Pauli	$12-16 \times 10^{-3}$	1.99	P2
$Li_{0.61}CoO_2$ [b]	$\propto T$	bad metal		16.6×10^{-3}	1.7	O3
$Na_{0.62}CoO_2$ [b]	$\propto T$	bad metal + spin entropy	Curie−Weiss	26.1×10^{-3}	2.02	P′3

[a] ρ (LT), resistivity at low temperature; α, thermopower; χ, magnetic susceptibility; γ, Sommerfeld coefficient. Complementary data are also provided for $Rb_{0.5}CoO_2$, $K_4Co_7O_{14}$, and $Na_{0.31}CoO_2$ and discussed in the text. [b] This work. [c] S. Nakamura et al. *J. Phys. Soc. Jpn.* **1999**, *68*, 3746. [d] M. Blangero et al. *Inorg. Chem.* **2005**, *44*, 9299−9304. [e] C.A. Marianetti et al. *Phys. Rev. Lett.* **2007**, *99*, 246404. [f] J.W Lynn et al. *Phys. Rev. B* **2003**, *68*, 214516.

gas, and we show that all our measurements betray an effective mass enhancement (m_χ, m_γ, m_α). We also show that their two-by-two comparison allows characterizing the diffusion mechanisms and reveals the enhancement of the electron correlations. We finally show that the more pronounced 2D character of this compound also implies a spin mass enhancement.

Numerous empirical expressions have been proposed to link these parameters; for a Fermi liquid, the comparison to the free electron model (sub/superscript "0") is given by[55,78−80]

$$\chi_e = \frac{m_\chi}{m_0(1-F^0)}\chi^0_{\text{Pauli}} \quad \text{with} \quad \chi^0_{\text{Pauli}} = \mu_B^2 g_0(E_F)\cdot\tilde{V} \quad (1)$$

$$\gamma = \frac{m_\gamma}{m_0}\gamma_0 \quad \text{with} \quad \gamma_0 = \left(\frac{\pi^2}{3}\right)k_B^2 g_0(E_F)\cdot\tilde{V} \quad (2)$$

$$\frac{|d\alpha(T)|}{dT} = \frac{m_\alpha}{m_0}\frac{|d\alpha_0(T)|}{dT} \quad \text{with} \quad \alpha_0(T) = \left(\frac{\pi^2 k_B^2}{3N_{Av}e(1-x)}\right)\left(1+\frac{2}{3}\zeta\right)g_0(E_F)\cdot\tilde{V} \quad (3)$$

m_χ, m_γ, and m_α are the effective masses calculated from magnetic, specific heat, and thermopower data, respectively; F^0 is the Landau parameter for a Fermi liquid and equals ~ -0.5 when the increase in χ^0_{Pauli} is only due to the increase of the effective mass;[79,81] ζ is the scattering exponent and $\tilde{V}$ is the molar volume used for unit conversion ($\tau \propto E^\zeta$; typical examples of ζ are $-1/2$ for acoustic phonon scattering, 0 for neutral impurity scattering, 1/2 for polar phonon or piezoelectric scattering or still 3/2 for charged impurity scattering). Assuming a spherical Fermi surface ($k_F = (3\pi^2 n)^{1/3}$), the density of state is given by $g_0(E_F) = 3n/2E_F$, n being the carrier density, and the Fermi energy is given by $E_F = \hbar^2 k_F^2/m_0$.[82] For an A_xCoO_2 phase, the carrier density is given by $n = (1-x)/(d_{Co-Co}{}^2 \times c \times \sqrt{3}/2)$ where $d_{Co-Co} = a$ and c are the crystal cell parameters. Table 9 gives the theoretical values calculated from expressions 1−3 for the free electron gas, together with the experimental values and the deduced effective masses (m_χ and m_γ; for the retrieval of m_α, an additional step based on the comparison of the thermopower slope to the Sommerfeld coefficient is necessary to first extract the scattering exponent as discussed in next paragraph). Wilson[83] has studied the R_w ratio between the Pauli susceptibility and the Sommerfeld coefficient to characterize Kondo systems:

$$R_W = \frac{\chi_{\text{Pauli}}}{\gamma}\left(\frac{\pi^2}{3}\frac{k_B^2}{\mu_B^2}\right) \quad (4)$$

In the case of the free electron gas, this ratio is 1 (Table 9) while it is up to 2 for the Kondo systems with highly correlated electrons.[84,85] The values obtained for the potassium phases are close to 2−3 and feature highly enhanced electron correlations. Such a high value was already observed in the case of $Na_{0.31}CoO_2$[98,86,87] and other oxides (Sr_2RuO_4;[88] $Sr_{1-x}La_xTiO_3$[89,90]).

Likewise, the thermopower slope can be related to the Sommerfeld coefficient.[91−93] Such a treatment, including the scattering exponent ζ, has recently been discussed by Behnia[80] in particular in the case of Na_xCoO_2. Taking into account the carriers' concentration, this relationship can be written as

$$q = \frac{|d\alpha(T)|}{dT}\frac{N_{Av}e}{\gamma} = \frac{1}{1-x}\left(1+\frac{2\zeta}{3}\right) \quad (5)$$

In the case of free electrons and of an energy-independent relaxation time ($\zeta = 0$), q is 1 for a system with one charge carrier per formula unit; it increases if the carrier concentration decreases. The q values calculated from the

(78) Georges, A.; Kotliar, G.; Krauth, W.; Rozenberg, M. J. *Rev. Mod. Phys.* **1996**, *68*, 13.
(79) Tokura, Y.; Taguchi, Y.; Okada, Y.; Fujishima, Y.; Arima, T.; Kumagai, K.; Iye, Y. *Phys. Rev. Lett.* **1993**, *70*, 2126.
(80) Behnia, K.; Jaccard, D.; Flouquet, J. *J. Phys.: Condens. Matter* **2004**, *28*, 5187.
(81) Rice, T. M. *Phys. Rev.* **1968**, *175*, 858.
(82) Ashcroft, N.W.; Mermin, N.D. *Solid state physics*; Holt, Rinehart, and Winston: New York, 1976.
(83) Wilson, K. G. *Rev. Mod. Phys.* **1975**, *47*, 773.
(84) Stewart, G. R.; Fisk, Z.; Willis, J. O.; Smith, J. L. *Phys. Rev. Lett.* **1984**, *52*, 679.
(85) Trainor, R. J.; Brodsky, M. B.; Culbert, H. V. *Phys. Rev. Lett.* **1975**, *34*, 1019.
(86) Yokoi, M.; Moyoshi, T.; Kobayashi, Y.; Soda, M.; Yasui, Y.; Sato, M.; Kakurai, K. *J. Phys. Soc. Jpn.* **2005**, *74*, 3046.
(87) Viciu, L.; Bos, J. W. G.; Zandbergen, H. W.; Huang, Q.; Foo, M. L.; Ishiwata, S.; Ramirez, A. P.; Lee, M.; Ong, N. P.; Cava, R. J. *Phys. Rev. B* **2006**, *73*, 174104.
(88) Maeno, Y.; Yoshida, K.; Hashimoto, H.; Nishizaki, S.; Ikeda, S.; Nohara, M.; Fujita, T.; Mackenzie, A. P.; Hussey, N. E.; Bednorz, J. G.; Lichtenberg, F. *J. Phys. Soc. Jpn.* **1997**, *66*, 1405.
(89) Trainor, R. J.; Brodsky, M. B.; Culbert, H. V. *Phys. Rev. Lett.* **1975**, *34*, 1019.
(90) Onoda, M.; Yasumoto, M. *J. Phys.: Condens. Matter* **1997**, *9*, 3861.
(91) Zlatic, V.; Rivier, N. *J. Phys. F: Met. Phys.* **1974**, *4*, 732.
(92) Zlatić, V.; Costi, T. A.; Hewson, A. C.; Coles, B. R. *Phys. Rev. B* **1993**, *48*, 16152.
(93) Merino, J.; McKenzie, R. H. *Phys. Rev. B* **2000**, *61*, 7996.

Table 9. Effective Mass of the Quasi-Particles in P2−$K_{0.61}CoO_2$ and P2−$K_4Co_7O_{14}$ Calculated from eqs 1−3. [a]

	P2−$K_4Co_7O_{14}$		P2−$K_{0.61}CoO_2$	
	Theoretical Values (Electron Gas)			
χ^0_{Pauli} ($\times 10^{-6}$ emu/mol)	19.6		19	
γ_0 (mJ/mol/K^2)	1.43		1.39	
$d\alpha_0/dT$ (nV/K^2)	34.6		36.9	
Rw_0	1		1	
q_0 $\zeta = 0$	7/3 = 2.33		2.56	
$\zeta = -1/2$	14/9 = 1.56		1.71	
$\zeta = 1$	35/9 = 3.89		4.27	
	Experimental Values (LT: Low Temperature < 50 K; HT: High Temperature > 120 K)			
χ_e ($\times 10^{-6}$ emu/mol)	302 ± 75		357 ± 52	
γ (mJ/mol/K^2)	8.8		9	
$\lvert d\alpha/dT \rvert$ (nV/K^2)	LT: 342	HT: 147	LT: 375	HT: 151
R_w	1.9−3.1		2.5−3.3	
q	LT: 3.75	HT: 1.61	LT: 4.02	HT: 1.62
	Effective Mass			
m_χ	23 ± 6		28 ± 4	
m_γ	6.2		6.5	
$m_{\alpha/T}$	LT: 5.9 ($\zeta = 1$)	HT: 6.4 ($\zeta = -1/2$)	LT: 6.1 ($\zeta = 1$)	HT: 6.1 ($\zeta = -1/2$)

[a] The Wilson and Benhia ratios are calculated from eqs 4 and 5, respectively. The uncertainties on the values of χ, Rw, and m_χ account for the uncertainty on the Van Vleck contribution.

experimental data are close to 4 at low temperature and to 1.6 at high temperature (Table 9). They are compatible with ζ values of 1 at low temperature and −0.5 at high temperature. Even though the model is strictly valid only at very low temperature, the high temperature value of ζ sounds reasonable if one keeps in mind that the dominant scattering process is expected to be due to acoustic phonons in this domain. Accounting for these values of ζ, the effective masses calculated from eq 3 are given in Table 9. $m_\alpha \sim 6$ and is very close to m_γ, but it is much smaller than the effective mass m_χ calculated from the magnetic susceptibility. This discrepancy could be explained by the enhanced two-dimensional character.

Terasaki et al. have evidenced the strong anisotropy of the electrical resistivity of single crystals of P2−$Na_{\sim 0.7}CoO_2$: along the *c* axis; it displays a maximum at $T^* \sim 180$ K while it remains metal-like in the (*ab*) plan; $\rho_c/\rho_{(ab)}$ is higher than 225 at 4 K. Valla et al.[94] have shown that the behavior was the one of a 3D metal for $T < T^*$ and the one of a 2D metal at higher temperature. A similar behavior was already observed for $(Bi_{0.5}Pb_{0.5})_2Ba_3Co_2O_y$,[95] the cuprate $TmBa_2Cu_3O_{6.37}$,[96] and the superconducting phase Sr_2RuO_4.[97] Rivadulla et al. have attributed this change in dimension to the anisotropic thermal expansion: while the expansion is negligible in the (*ab*) plane, the one along *c* fast increases above T^*, which decreases the interactions between the CoO_2 layers. For $x \sim 0.6$, the in-plane and out-of-plane cobalt−cobalt interactions should be lower for the potassium phases as compared to the sodium one because (Tables 3−5) (i) d_{Co-Co} slightly decreases ($\Delta a \sim 0.7\%$); (ii) *c* largely increases ($\Delta c \sim 13\%$). The physical properties of K_xCoO_2 ($x \sim 0.6$) are actually closer to the ones of Na_xCoO_2 ($x < 0.5$) that also exhibit a resistivity typical of a metal and a T^2 domain at low temperature, and a nearly temperature independent magnetic susceptibility.[98] The *c*/*a* ratio (~4.34) is close to the one of $Na_{0.31}CoO_2$ and indeed suggests a more pronounced 2D character (the P2−$Rb_{\sim 0.5}CoO_2$ phase[99] that has an even larger *c*/*a* ratio exhibits a conventional metal behavior).

Qian et al. have recently calculated for a 2D electron gas the enhancement of the effective mass due to spin correlations in electron liquids.[100] Owing to their results, the ratio of the band to quasiparticle masses is close to one while the one of the spin to the quasiparticle masses can be very high depending on the magnitude of the spin correlations. Using a Wigner radius $r_{s\text{-}2D} = 4.6$ Å for the ordered and $r_{s\text{-}2D} = 4.8$ Å for the disordered phases, m_χ/m_γ is extrapolated to, respectively, 4.7 and 4.9; using the values of m_γ given in Table 9, the spin mass enhancement can then be estimated to about 28 and 30, respectively, in reasonable agreement with the values calculated from the susceptibility data.

The low temperature value of the scattering exponent ζ, as well as the change in sign of the thermopower still remain unclear but they suggest a complex diffusion process. We propose two different scenarios both compatible with our data, but mainly based on the change in sign of the thermopower. The first one is after the work of Merino et al.[91] These authors have calculated for a strongly correlated Fermi liquid (with $U/t \sim 2-3$) a progressive evolution with increasing temperature from

(94) Valla, T.; Johnson, P. D.; Yusof, Z.; Wells, B.; Li, Q.; Loureiro, S. M.; Cava, R. J.; Mikami, M.; Mori, Y.; Yoshimura, M.; Sasaki, T. *Nature* **2002**, *417*, 627.
(95) Loureiro, S. M.; Young, D. P.; Cava, R. J.; Jin, R.; Liu, Y.; Bordet, P.; Qin, Y.; Zandbergen, H.; Godinho, M.; Núñez Regueiro, M.; Batlogg, B. *Phys. Rev. B* **2001**, *63*, 94109.
(96) Lavrov, A. N.; Kameneva, M. Y.; Kozeeva, L. P. *Phys. Rev. Lett.* **1998**, *81*, 5636.
(97) Maeno, Y.; Yoshida, K.; Hashimoto, H.; Nishizaki, S.; Ikeda, S.; Nohara, M.; Fujita, T.; Mackenzie, A. P.; Hussey, N. E.; Bednorz, J. G.; Lichtenberg, F. *J. Phys. Soc. Jpn.* **1997**, *66*, 1405.
(98) Foo, M. L.; Wang, Y.; Watauchi, S.; Zandbergen, H. W.; He, T.; Cava, R. J.; Ong, N. P. *Phys. Rev. Lett.* **2004**, *92*, 247001.
(99) Nakamura, S.; Ozawa, A. *J. Phys. Soc. Jpn.* **1999**, *68*, 3746.
(100) Qian, Z.; Vignale, G.; Marinescu, D. C. *Phys. Rev. Lett.* **2004**, *93*, 106601.

coherent to incoherent quasiparticles excitations. The thermal destruction of the coherence is associated with a maximum in the thermopower and the specific heat, and the end of the T^2 domain of the resistivity; the maximum in the specific heat can however be hidden by the lattice contribution. In this model, the low temperature slope of the thermopower scales as the effective mass. A second scenario relies on the electron−phonon coupling and the possible existence of a phonon-drag peak in the thermopower.[101,102] This peak is expected to appear at $0.1-0.2 \times \theta_D = 40-80$ K[93,103] which is close to the values obtained for the minimum of the thermopower (60 and 75 K for respectively the ordered and the disordered phases).

Sodium Phase, a Spin Polarized Behavior. The properties of P′3−$Na_{0.62}CoO_2$ can be summarized as follows: (i) the resistivity linearly increases with temperature (Figure 8); (ii) the thermopower increases with temperature and tends to saturate at high temperature (Figure 10); (iii) the magnetic susceptibility is of Curie−Weiss type (Figures 11, 12) in agreement with the magnetic phase diagram of the system P2−Na_xCoO_2 for $x > 0.5$; the Curie constant is consistent with the Co^{4+} content deduced from the nominal composition; $|\theta_p|$ is large suggesting strong electron correlations; (iv) specific heat measurements (Figure 13) reveal a high value of the Sommerfeld coefficient (26.1 mJ/mol K^2) confirming the presence of strong electron correlations; in addition, an anomaly is clearly visible at about 350 K that has been attributed to the sodium mobility in the interslab.[31]

The sodium system has been the subject of extensive reports during the past few years. However, the origin of the high thermopower in Na_xCoO_2 ($x > 0.5$) is still debated and would arise from the enhancement of the effective mass due to the electron correlations[4,104] or from the entropy excess of carriers occupying degenerate states.[105] Limelette et al.[72] have provided some arguments in favor of a coexistence of both contributions in the misfit cobalt multiple oxides with a rocksalt interslab $[Ca_2CoO_3]_{0.62}[CoO_2]$ and $[Bi_{1.7}Co_{0.3}Ca_2O_4]_{0.6}CoO_2$. We may additionally note that there is still a controversy concerning the possible oxygen non-stoichiometry in this family of materials and in particular for the sodium phases,[24−28] and we cannot exclude, though unclear, that it can have a significant effect on the properties we observe.

Unlike the potassium phases that display Pauli paramagnetism, the Curie−Weiss dependence of the magnetic susceptibility of the sodium phase is in agreement with the behavior of spin polarized holes. This can lead to a spin entropy contribution to the thermopower of the order[49] of $\alpha_S = (k_B/e) \ln(2)$ ($\approx 60\ \mu$V/K). Figure 14 shows the temperature dependence of the thermopower difference between P′3−$Na_{0.62}CoO_2$ and the other systems.

This plot evidences an asymptotic regime for $T > 150$ K with a value at 300 K ranging from 40 to 55 μV/K. Note that the same kind of result can be obtained[25] by subtracting the data of Na_xCoO_2 with $x < 0.5$ from that of Na_xCoO_2 with $x > 0.5$. One can see that the spin

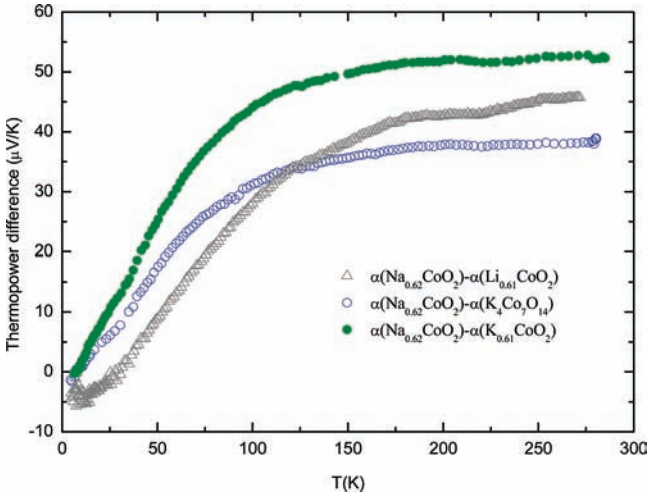

Figure 14. Temperature dependence of the thermopower difference between P′3−$Na_{0.62}CoO_2$ and O3−$Li_{0.61}CoO_2$, P2−$K_4Co_7O_{14}$,[17] and P2−$K_{0.61}CoO_2$.

contribution to the thermopower at 300 K reaches 67 to 92% of α_S, depending on the reference chosen, but anyway suggesting a major contribution of the spin entropy for $Na_{0.62}CoO_2$. Additionally, the thermopower slope is larger than for a conventional metal, and the high value of the Sommerfeld coefficient also reveals a strong enhancement of the effective mass. We thus suggest, as already proposed by Limelette et al.,[72] that the increase of the thermopower for this system is also due to the quasiparticles' effective mass enhancement which is reinforced by a large spin entropy contribution. This simple treatment actually also suggests that the intrinsic behavior of all three compounds is very close: removing the progressive spin entropy contribution to the sodium phase, all these alkali cobalt double oxides offer a similar temperature dependence, the thermopower being negative at low temperature and then increasing and crossing 0 to finally be positive at higher temperature. The origin of this behavior and especially the change in sign is still unclear.

Lithium Phase, an Intermediate Behavior. The behavior of the O3−$Li_{0.61}CoO_2$ phase looks more complex. It displays a temperature dependence of the resistivity similar to that of the sodium phase (Figure 8), several regimes for the thermopower (Figure 10), a complex magnetic behavior with a T-hysteresis in the magnetization data (Figures 11, 12), and a jump in the specific heat (Figure 13). The change in regimes appears in the same temperature range for the thermopower (Figure 10, inset) and the magnetization (Figure 11, inset), and is associated to the jump in the specific heat (Figure 13); however, the resistivity is not affected by this transition. As already mentioned, we suggest that this transition is associated with the freezing of Li^+ ions at low temperature as already observed in P′3−$Na_{0.62}CoO_2$;[31] the ionic contribution to the resistivity being expected to be much less than the electronic one, it is fully masked at a macroscopic scale and is not visible with the resistivity measurements. In addition, the effect of freezing the alkali mobility on the phonon scattering of the itinerant holes moving in the CoO_2 layers cannot be simply anticipated. Since the Sommerfeld coefficient is intermediate between the one of the potassium phase and the one of the sodium phase

(101) Jonson, M.; Mahan, G. D. *Phys. Rev. B* **1990**, *42*, 9350.
(102) Huebener, R. P. *Phys. Rev.* **1966**, *146*, 502.
(103) Weiss, J. D.; Lazarus, D. *Phys. Rev. B* **1974**, *10*, 456.
(104) Pálsson, G.; Kotliar, G. *Phys. Rev. Lett.* **1998**, *80*, 4775.
(105) Koshibae, W.; Maekawa, S. *Phys. Rev. Lett.* **2003**, *91*, 257003.

($9 < 16.6 < 26.1$ mJ/mol K^2), we suggest that it actually has an intermediate behavior due to intermediate electron correlations.

Conclusion

Three lamellar cobalt double oxides A_xCoO_2 ($x \sim 0.6$) with A = Li, Na, K have been synthesized; they crystallize in the O3, P′3, and P2 systems, respectively. In spite of clear structural differences, the correlation of the very different electronic properties to the structural features is not straightforward. All these materials exhibit strong electron correlations that are increasing from the potassium to the sodium phase. The three phases are metallic like, but while for the potassium phase the electrical resistivity shows a low temperature T^2 dependence, for the lithium and sodium phases it linearly decreases as the temperature is lowered, at least down to 4 K. The Seebeck coefficient remains low for both the lithium and the potassium phases whereas it is enhanced by a large spin entropy contribution in the sodium case. The magnetic behavior of the lithium phase seems complex, but it appears Pauli-like for P2−$K_{0.61}CoO_2$ and of Curie−Weiss type for P′3−$Na_{0.62}CoO_2$. The Sommerfeld coefficient increases from Li to K and Na phases. For the sodium case, these results lead to consider a spin polarized system with a large particles' effective mass enhancement and a spin entropy contribution. The potassium phase presents characteristics close to those of the Na_xCoO_2 system for poor sodium rates ($x < 0.5$) and actually looks very close to a 2D system. Two scenarios are proposed that agree with the observed low temperature properties: (i) the thermal destruction of the coherence of quasiparticles excitations and (ii) an electron−phonon coupling with a phonon-drag peak in the thermopower. The lithium case is more complex and offers an intermediate behavior with a middle Sommerfeld coefficient, a resistivity closer to that of the sodium phase, a thermopower closer to that of the potassium phase, and a complex behavior of the magnetization.